JACS
JOURNAL OF THE AMERICAN CHEMICAL SOCIETY
Communication
pubs.acs.org/JACS

Ratio-Controlled Synthesis of CuNi Octahedra and Nanocubes with Enhanced Catalytic Activity

Menglin Wang,[‖] Liangbing Wang,[‖] Hongliang Li, Wenpeng Du, Munir Ullah Khan, Songtao Zhao, Chao Ma, Zhenyu Li, and Jie Zeng*

Hefei National Laboratory for Physical Sciences at the Microscale, CAS Centre for Excellence and Synergetic Innovation Centre in Quantum Information and Quantum Physics, Center of Advanced Nanocatalysis (CAN-USTC), Department of Chemical Physics, University of Science and Technology of China, Hefei, Anhui 230026, P. R. China

Supporting Information

ABSTRACT: Non-noble bimetallic nanocrystals (NCs) have been widely explored due to not only their low cost and abundant content in the Earth's crust but also their outstanding performance in catalytic reactions. However, controllable synthesis of non-noble alloys remains a significant challenge. Here we report a facile synthesis of CuNi octahedra and nanocubes with controllable shapes and tunable compositions. Its success relies on the use of borane morpholine as a reducing agent, which upon decomposition generates a burst of H_2 molecules to induce rapid formation of the nuclei. Specifically, octahedra switched to nanocubes with an increased amount of borane morpholine. In addition, the ratio of CuNi NCs could be facilely tuned by changing the molar ratio of both precursors. The obtained CuNi NCs exhibited high activity in aldehyde-alkyne-amine coupling reactions, and their performance is strongly facet- and composition-dependent due to the competition of the surface energy (enhanced by increasing the percent of Ni) and active sites (derived from Cu atoms).

Metal nanocrystals (NCs) have received considerable interest due to their remarkable performance in catalytic reactions including oxidation, cross-coupling, and hydrogenation.[1,2] It is well-known that the activity and selectivity of metal NCs for a certain catalytic reaction can be optimized by controlling the elemental composition and the type of exposed facets.[3,4] To this end, a wide variety of methods have been developed to synthesize NCs with well-defined compositions and specific enclosed facets. However, to our knowledge, most reported NCs are noble metals, such as Pt, Pd, Au, and Ag. There are limited reports on controllable synthesis of non-noble metals (Cu, Fe, Co, and Ni), despite their low cost and abundant content in the Earth's crust. Since the reduction potentials of non-noble metals are generally much lower than those of noble metals,[5] more strenuous reaction conditions are required to reduce non-noble metal precursors, and to form alloys, the differences in reduction potentials between different metals must be eliminated. Further, the relatively high susceptibility of non-noble metal NCs upon exposure to solution and air makes it very difficult to obtain ideal shapes with specific enclosed facets. Fe nanocubes and nanoframes with high uniformity were prepared by setting the reduction temperature as high as 380 °C.[6] Well-defined Ni nanocubes were also prepared using trioctylphosphine as a capping agent to regulate the morphology.[7] Besides traditional wet chemical reduction, electrochemical reduction has been applied to prepare bimetallic FeNi concave nanocubes and nanocages with high-index facets.[8] Although several synthetic systems have been developed, controlled synthesis of non-noble metal NCs is still in a rudimentary state relative to what has been achieved for noble metals.

Here we report a facile synthesis of single-crystal CuNi NCs with controllable shapes and tunable compositions. Its success largely relies on the use of borane morpholine as a reducing agent, which upon decomposition generates a burst of H_2 molecules to induce the rapid formation of the nuclei. Further, the morphology of the CuNi NCs changes from octahedra to nanocubes with an increased amount of borane morpholine. The Cu/Ni ratio could be tuned simply by varying the initial molar ratios of precursors. The obtained CuNi NCs are employed as catalysts for the aldehyde-alkyne-amine (A^3) coupling reaction to investigate their shape- and composition-dependent catalytic activities; $Cu_{50}Ni_{50}$ nanocubes achieved the highest activity. Based on theoretical calculations, the activity of catalysts is closely associated with the competition of surface energy (enhanced by the increase of Ni atoms) and active sites (derived from Cu atoms).

In a typical synthesis, $Cu(acac)_2$ and $Ni(acac)_2$ were dissolved in a solution containing diphenyl ether, oleylamine, and oleic acid. The mixture was preheated in an oil bath at 240 °C for 5 min, and 20 mg of borane morpholine complex was added. CuNi octahedra were obtained after the reaction proceeded for 30 min and the solution cooled to room temperature. Figure 1A,B shows representative high-angle annular dark-field scanning transmission electron microscopy (HAADF-STEM) images of the obtained CuNi octahedra with an average edge length of 14.5 nm (Figure S1), indicating formation of an octahedral shape in high purity and with good size uniformity. High-resolution transmission electron microscopy (HRTEM) of an individual NC clearly reveals the single-crystal structure of CuNi octahedra with a lattice parameter of 2.1 Å (Figure 1C). This image, recorded along the [110] zone axis, is substantiated by the corresponding Fourier transform (FT) pattern provided in the inset. As shown in Figure 1D, X-ray diffraction (XRD) peaks of the CuNi octahedra all lie among the peak positions of pure Cu and Ni.

Received: August 6, 2015
Published: October 24, 2015

DOI: 10.1021/jacs.5b08289
J. Am. Chem. Soc. 2015, 137, 14027−14030

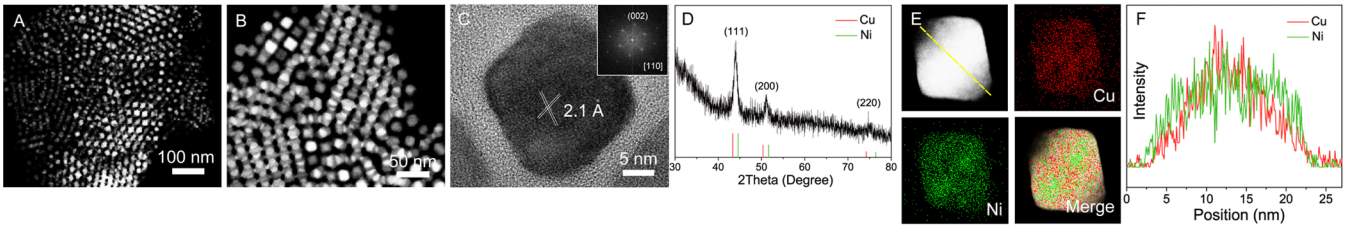

Figure 1. (A,B) HAADF-STEM images of CuNi alloy octahedra. (C) HRTEM image of an individual CuNi alloy octahedron; inset is the corresponding FT pattern. (D) XRD pattern of CuNi alloy octahedra. (E) STEM image and STEM-EDX elemental mapping of an individual CuNi octahedron. (F) Compositional line profile of Cu and Ni from a CuNi octahedron recorded along the line shown in the STEM image. Red = Cu; green = Ni.

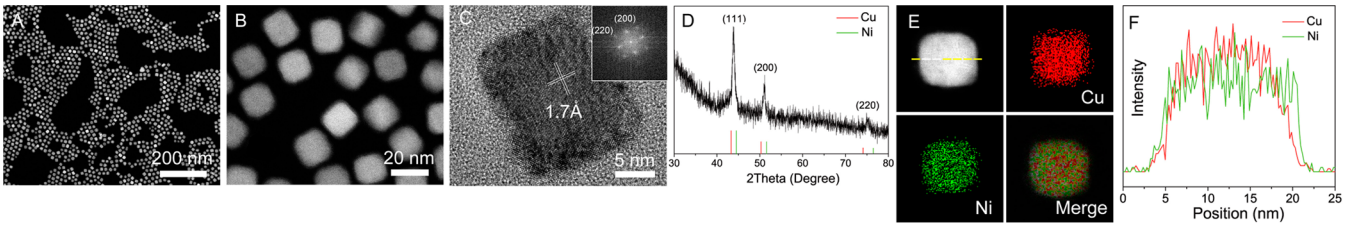

Figure 2. (A,B) HAADF-STEM images of CuNi alloy nanocubes. (C) HRTEM image of an individual CuNi alloy nanocube; inset is the corresponding FT pattern. (D) XRD pattern of CuNi alloy nanocubes. (E) STEM image and STEM-EDX elemental mapping of an individual CuNi nanocube. (F) Compositional line profile of Cu and Ni from a CuNi nanocube recorded along the line shown in the STEM image. Red = Cu; green = Ni.

Based on Vegard's law,[9] which claims a linear relation between the lattice parameter of an alloy and its composition, the content of Cu in CuNi octahedra was estimated to be ~50%. To analyze the structure and elemental composition of the nanostructure, STEM-energy dispersive X-ray (EDX) elemental mapping images of an individual NC are presented in Figure 1E, indicating that both Cu and Ni are homogeneously distributed throughout the NC. The cross-sectional compositional line-scanning profile of the octahedron in Figure 1F further proves the complete overlap of both elements without significant segregation of each component. The above analysis confirms the successful preparation of CuNi alloy octahedra. As revealed by inductively coupled plasma-atomic emission spectroscopy (ICP-AES), the atomic percentage of Cu was 51%, well consistent with the ratio of precursors supplied. Further experiment reveals that nearly all the metal precursors (>95%) were reduced within 15 min, based on ICP-AES data of Cu and Ni remaining in the solution (Figure S2A).

The synthetic protocol for preparing CuNi nanocubes was similar to that of CuNi octahedra, except the amount of borane morpholine was increased to 40 mg (Figure 2A,B). The edge length decreased to 12.8 nm (Figure S1). The HRTEM image and corresponding FT pattern recorded along the [001] zone axis indicate that the CuNi nanocube was a single crystal with lattice parameter of 1.7 Å (Figure 2C). As for the $Cu_{51}Ni_{49}$ octahedra, XRD, STEM-EDX, compositional line-scanning, and ICP-AES (Figures 2D–F and S2B) of CuNi nanocubes consistently support the alloy structures having 50% Cu.

A key to the synthesis of non-noble metal NCs with well-defined shapes is to select an appropriate reducing agent. In our synthetic systems, no product was obtained when 1-octadecylene or oleylamine was used as reducing agent. In high-temperature pyrolysis, products containing both single-crystal and twinned $Cu_{95}Ni_5$ NCs were obtained with a broad size distribution, 5–45 nm (Figures S3 and S4). In this work, borane morpholine was applied since its strong reducing power could guarantee complete reduction of precursors. Essentially, the reducing role was played by H_2 generated upon decomposition of borane morpholine. Based on the time profile for H_2 generation (Figure S5), the amount of H_2 increased initially and reached its maximum within 10 s. Such explosive generation of H_2 could lead to fast reduction and thus formation of more nuclei at the initial stage. Later in the reaction, most of the reducing agent was consumed, retarding the growth of seeds. As a result, CuNi nanocubes with a small and uniform size (<15 nm) were obtained, owing to rapid formation of nuclei with a high concentration, followed by relatively slow growth of seeds. For comparison, we conducted a control experiment with directly blowing H_2, under which a relatively slow reduction rate and a decreased number of seeds were obtained in the early stage, forming larger CuNi NCs, >100 nm (Figure S6). In both cases, H_2 provided a reducing atmosphere that effectively prevented re-oxidation of metal atoms. It is worth pointing out that the morphology of the final product is also sensitive to the amount of borane morpholine. With a relatively small amount of borane morpholine (20 mg) added, the NCs tended to possess octahedral morphology enclosed by (111) facets, while nanocubes bounded by (100) facets were generated when the amount of borane morpholine was increased to 40 mg. A similar phenomenon was observed when we used borane-*tert*-butylamine complex instead of borane morpholine. Specifically, octahedra were replaced by nanocubes with increasing amount of borane-*tert*-butylamine complex (Figure S7).

We proposed a possible mechanism to explain the observed facet selectivity. Specifically, since (111) facets enjoy the lowest surface energy for a face-centered cubic structure, the formation of octahedra, with maximized expression of (111) facets, is thermodynamically favorable to reduce the total surface energy. Notably, the products took a cubic instead of octahedral morphology when the amount of borane morpholine was increased from 20 to 40 mg (Figures 1, 2, and S8). One possible explanation for this phenomenon is that some chemicals derived from borane morpholine (maybe H_2 molecules or morpholine) in the synthetic systems act as capping agents and selectively adsorb onto the (100) facets, making these facets thermodynamically more favorable by reducing their interfacial free energies through chemisorption. This is partly supported by the shape evolution process for CuNi octahedra and nanocubes shown in

DOI: 10.1021/jacs.5b08289
J. Am. Chem. Soc. 2015, 137, 14027–14030

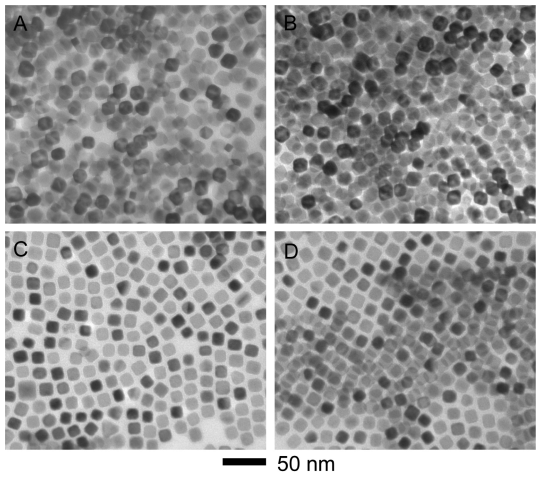

Figure 3. TEM images of (A) $Cu_{35}Ni_{65}$ octahedra, (B) $Cu_{67}Ni_{33}$ octahedra, (C) $Cu_{33}Ni_{67}$ nanocubes, and (D) $Cu_{66}Ni_{34}$ nanocubes.

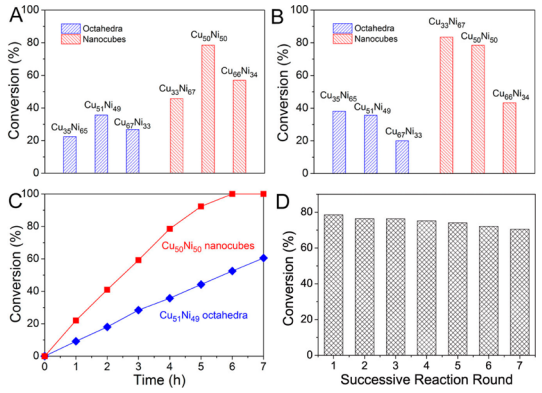

Figure 4. (A,B) Conversion toward A^3 coupling using CuNi catalysts with 1% mass loading of total metal and 0.5% mass loading of Cu. (C) Conversion as a function of time for $Cu_{51}Ni_{49}$ octahedra and $Cu_{50}Ni_{50}$ nanocubes. (D) Relative activity of $Cu_{50}Ni_{50}$ nanocubes over the course of seven rounds of successive reaction.

Figure S9: CuNi octahedra evolve from cuboctahedral and truncated octahedral seeds due to the thermodynamic control. In comparison, the increased amount of borane morpholine induces formation of nanocubes from similar seeds, since sufficient capping agents derived from borane morpholine adsorb onto (100) facets, leading to more expression of these facets (Figure S10).

The Cu/Ni ratio of the resultant NCs was also investigated by simply varying the original molar ratios of precursors using the same synthetic procedure. Based on ICP-AES analysis, the Cu/Ni atomic ratios in the products were in good agreement with those in the initial precursors. As revealed by TEM images (Figure 3), for the case of CuNi octahedra, when the Cu/Ni ratio of precursors was changed, the resultant products, $Cu_{35}Ni_{65}$ and $Cu_{67}Ni_{33}$, had high crystallinity and purity with basically unchanged morphology. Similarly, the obtained $Cu_{33}Ni_{67}$ and $Cu_{66}Ni_{34}$ nanocubes were monodisperse and highly crystalline. These observations indicate that tuning the molar ratio of precursors within a proper range yielded NCs with varied compositions without greatly changing the morphology, and the molar ratio of products corresponded well to that of the precursors. Although the reduction potential of Cu^{2+}/Cu^0 (0.34 V vs RHE) is far more positive than that of Ni^{2+}/Ni^0 (−0.21 V vs RHE), the involvement of oleylamine narrowed the gap in the reduction potential between the two metal precursors due to coordination of oleylamine with metal ions, resulting in co-reduction of Cu^{2+} and Ni^{2+} to form an alloy structure.[10] When only Cu or Ni precursors were added in the standard procedure for CuNi octahedra and nanocubes, irregular NCs were obtained and used for later comparison in catalysis, indicating that formation of well-defined NCs with specific facets is also related to the combination of Cu and Ni (Figure S11).

Synthesis of single-crystal CuNi octahedra and nanocubes with tunable ratios provides an ideal platform to investigate the dependence of catalytic activity on the facets and composition. Coupling of alkyne, aldehyde, and amine—A^3 coupling—was chosen as a model reaction to explore the catalytic performance of CuNi NCs.[11] CuNi NCs were loaded on active carbon without further treatment. Based on X-ray photoelectron spectroscopy, the majority of surface metal atoms were not capped by surfactant such as oleylamine and oleic acid (Figure S12). To determine the active element in this reaction, we benchmarked the catalytic activities of CuNi NCs against Cu and Ni NCs toward A^3 coupling (Table S1). It is clearly seen that Ni was inactive, while Cu catalyzed this reaction with ∼15% conversion, indicating that Cu serves as the active element. In Figure 4A, we compare the catalytic performance of octahedra and nanocubes with different Cu/Ni ratios (1% mass loading of total metal). Under the same reaction conditions (4 h, 120 °C), the catalytic activity of nanocubes is always higher than that of octahedra at the same composition, and the activity of NCs enclosed by the same facet was optimized when the molar ratio of Cu was ∼50% (Table S2). The conversion of this reaction using $Cu_{50}Ni_{50}$ nanocubes was 2.2 times that of the reaction using $Cu_{51}Ni_{49}$ octahedra, reaching 78.5%.

To further investigate the roles of facets and composition in catalysis, the catalytic activities were normalized to the intrinsic turnover frequency (TOF). The TOFs of CuNi nanocubes were much higher than those of CuNi octahedra, maximizing at 2953 h^{-1} for CuNi nanocubes (Figure S13A). When we used catalysts with the same Cu mass loading, the catalytic activity of nanocubes was always higher than that of octahedra at the same composition, and the activity increased with increasing Ni content for catalysts with the same facet (Table S3, Figures 4B and S13B). Conversion during the reaction is illustrated in Figure 4C, showing that when $Cu_{50}Ni_{50}$ nanocubes were used as catalyst, the conversion was almost 100% after 6 h of reaction. By comparison, the conversion was only 52.5% after 6 h with $Cu_{51}Ni_{49}$ octahedra as catalyst.

To explore the leaching behaviors of CuNi NCs, we measured the concentration of Cu and Ni in the filtrate of all CuNi catalysts after catalytic reaction (Table S4). The concentrations of Cu species in the reaction filtrate were elevated with increasing Cu ratios of CuNi NCs and were ∼10−50 ppb, less than 0.2% of the amount supplied. Hence, the amount of Cu species leached in CuNi NCs with different ratios was not consistent with their corresponding catalytic activity. When the reaction filtrates were allowed to react at 120 °C for an additional 4 h without catalysts, the reaction barely proceeded further (Table S5). Consequently, A^3 coupling in our catalytic system was majorly catalyzed heterogeneously on the surface of CuNi NCs. In addition, the stability of $Cu_{50}Ni_{50}$ nanocubes was studied by performing successive rounds of reaction (Figure 4D). After seven rounds, almost 90% of the original activity was preserved, showing high stability of $Cu_{50}Ni_{50}$ nanocubes. TEM (Figure S14) reveals that

DOI: 10.1021/jacs.5b08289
J. Am. Chem. Soc. 2015, 137, 14027−14030

these nanocubes maintained their morphology after catalytic reaction.

To elucidate the genesis of the differences in catalytic activity among CuNi NCs with different exposed facets and compositions, density functional theory calculations were performed, investigating the surface energy of CuNi NCs modeled in Figure S15. The surface energy of the (111) facet increases with increasing ratio of Ni atoms in CuNi alloy, minimizing at 0.091 eV/Å^2 for bulk Cu and maximizing at 0.138 eV/Å^2 for pure Ni (Figures 4B and S16). The surface energy of the (100) facet shows a similar trend but is always higher than that of the (111) facet at the same molar ratio. Considering that there is a positive correlation between surface energy and catalytic activity,[12] CuNi nanocubes are supposed to exhibit a higher activity than CuNi octahedra with the same molar ratio (Figure S16 and Table S6). Introducing Ni atoms contributes greatly to the enhancement of catalytic activity enclosed by the same facet, supported by catalytic experiments conducted with the same Cu mass loading (Figure 4B and Table S3). However, excessive Ni atoms will decrease the atomic percentage of Cu, which could provide accessible catalytically active sites for A^3 coupling, and accordingly decrease the catalytic activity. Hence, it is comprehensible that activity in this reaction is a volcano-type model as a function of Cu/Ni ratios. Taking surface energy and active sites into account, we can conclude that the high activity of $Cu_{50}Ni_{50}$ nanocubes could be associated with the optimum of high surface energy and sufficient exposed active sites.

In conclusion, we have synthesized CuNi octahedra and nanocubes with controllable ratios. The key was to employ borane morpholine as a reducing agent, the decomposition of which led to the explosive generation of H_2 molecules. Typically, the morphology of CuNi nanocrystals changes from octahedra to nanocubes with increasing amount of borane morpholine. The Cu/Ni ratios are varied simply by changing the molar ratio of precursors. Our study reveals that the catalytic performance for the A^3 coupling reaction depends on the morphology and composition of the catalysts. Further theoretical analysis shows that the best catalytic performance of $Cu_{50}Ni_{50}$ nanocubes could be related to high surface energy and sufficient active sites. This approach not only paves the way for rational design and synthesis of non-noble metal nanocrystals with controllable shapes and tunable compositions but also advances our understanding of the facet- and composition-dependent catalytic properties.

■ ASSOCIATED CONTENT

Supporting Information

The Supporting Information is available free of charge on the ACS Publications website at DOI: 10.1021/jacs.5b08289.

Experimental details; Figures S1−S16; Tables S1−S6 (PDF)

■ AUTHOR INFORMATION

Corresponding Author

*zengj@ustc.edu.cn

Author Contributions

‖M.W. and L.W. contributed equally.

Notes

The authors declare no competing financial interest.

■ ACKNOWLEDGMENTS

This work was supported by Collaborative Innovation Center of Suzhou Nano Science and Technology, MOST of China (2014CB932700), 2015SRG-HSC049, NSFC (grants 21222304, 21421063, 21203173, 21573206, 51371164, 51132007, and J1030412), Strategic Priority Research Program B of the CAS (XDB01020000), and Fundamental Research Funds for the Central Universities (WK2340000050, WK206-0190025, and WK3510000002).

■ REFERENCES

(1) (a) Huang, X.; Zhao, Z.; Cao, L.; Chen, Y.; Zhu, E.; Lin, Z.; Li, M.; Yan, A.; Zettl, A.; Wang, Y. M.; Duan, X.; Mueller, T.; Huang, Y. *Science* **2015**, *348*, 1230. (b) Xiao, B.; Niu, Z.; Wang, Y.-G.; Jia, W.; Shang, J.; Zhang, L.; Wang, D.; Fu, Y.; Zeng, J.; He, W.; Wu, K.; Li, J.; Yang, J.; Liu, L.; Li, Y. *J. Am. Chem. Soc.* **2015**, *137*, 3791. (c) Wang, L.; Zhao, S.; Liu, C.; Li, C.; Li, X.; Li, H.; Wang, Y.; Ma, C.; Li, Z.; Zeng, J. *Nano Lett.* **2015**, *15*, 2875. (d) Motl, N. E.; Smith, A. F.; DeSantis, C. J.; Skrabalak, S. E. *Chem. Soc. Rev.* **2014**, *43*, 3823.

(2) (a) Zhu, W.; Zhang, Y.-J.; Zhang, H.; Lv, H.; Li, Q.; Michalsky, R.; Peterson, A. A.; Sun, S. *J. Am. Chem. Soc.* **2014**, *136*, 16132. (b) He, R.; Wang, Y.; Wang, X.; Wang, Z.; Liu, G.; Zhou, W.; Wen, L.; Li, Q.; Wang, X.; Chen, X.; Zeng, J.; Hou, J. G. *Nat. Commun.* **2014**, *5*, 4327. (c) Li, C.; Jiang, B.; Imura, M.; Malgras, V.; Yamauchi, Y. *Chem. Commun.* **2014**, *50*, 15337. (d) Yin, X.; Liu, X.; Pan, Y.-T.; Walsh, K. A.; Yang, H. *Nano Lett.* **2014**, *14*, 7188. (e) Chiu, C.-Y.; Chen, C.-K.; Chang, C.-W.; Jeng, U.-S.; Tan, C.-S.; Yang, C.-W.; Chen, L.-J.; Yen, T.-J.; Huang, M. H. *J. Am. Chem. Soc.* **2015**, *137*, 2265.

(3) (a) Quan, Z.; Xu, H.; Wang, C.; Wen, X.; Wang, Y.; Zhu, J.; Li, R.; Sheehan, C. J.; Wang, Z.; Smilgies, D. M.; Luo, Z.; Fang, J. *J. Am. Chem. Soc.* **2014**, *136*, 1352. (b) Brodsky, C. N.; Young, A. P.; Ng, K. C.; Kuo, C.-H.; Tsung, C.-K. *ACS Nano* **2014**, *8*, 9368. (c) Zhang, S.; Hao, Y.; Su, D.; Doan-Nguyen, V. V. T.; Wu, Y.; Li, J.; Sun, S.; Murray, C. B. *J. Am. Chem. Soc.* **2014**, *136*, 15921. (d) Zhao, X.; Chen, S.; Fang, Z.; Ding, J.; Sang, W.; Wang, Y.; Zhao, J.; Peng, Z.; Zeng, J. *J. Am. Chem. Soc.* **2015**, *137*, 2804.

(4) (a) Kim, D.; Resasco, J.; Yu, Y.; Asiri, A. M.; Yang, P. *Nat. Commun.* **2014**, *5*, 4948. (b) Chen, S.; Su, H.; Wang, Y.; Wu, W.; Zeng, J. *Angew. Chem., Int. Ed.* **2015**, *54*, 108. (c) Wang, F.; Li, C.; Chen, H.; Jiang, R.; Sun, L.-D.; Li, Q.; Wang, J.; Yu, J. C.; Yan, C.-H. *J. Am. Chem. Soc.* **2013**, *135*, 5588. (d) Gao, C.; Hu, Y.; Wang, M.; Chi, M.; Yin, Y. *J. Am. Chem. Soc.* **2014**, *136*, 7474. (e) Moon, G. D.; Lim, G. H.; Song, J. H.; Shin, M.; Yu, T.; Lim, B.; Jeong, U. *Adv. Mater.* **2013**, *25*, 2707.

(5) Housecroft, C.; Sharpe, A. G. *Inorganic Chemistry*; Prentice Hall: Englewood Cliffs, NJ, 2012.

(6) Kim, D.; Park, J.; An, K.; Yang, N. K.; Park, J. G.; Hyeon, T. *J. Am. Chem. Soc.* **2007**, *129*, 5812.

(7) LaGrow, A. P.; Ingham, B.; Cheong, S.; Williams, G. V. M; Dotzler, C.; Toney, M. F.; Jefferson, D. A.; Corbos, E. C.; Bishop, P. T.; Cookson, J.; Tilley, R. D. *J. Am. Chem. Soc.* **2012**, *134* (134), 855.

(8) Moghimi, N.; Abdellah, M.; Thomas, J. P.; Mohapatra, M.; Leung, K. T. *J. Am. Chem. Soc.* **2013**, *135*, 10958.

(9) Denton, A. R.; Ashcroft, N. W. *Phys. Rev. A: At., Mol., Opt. Phys.* **1991**, *43*, 3161.

(10) (a) Xia, B. Y.; Wu, H. B.; Wang, X.; Lou, X. W. *J. Am. Chem. Soc.* **2012**, *134*, 13934. (b) Xia, B. Y.; Wu, H. B.; Li, N.; Yan, Y.; Lou, X. W.; Wang, X. *Angew. Chem., Int. Ed.* **2015**, *54*, 3797. (c) Zhang, L.; Su, H.; Sun, M.; Wang, Y.; Wu, W.; Yu, T.; Zeng, J. *Nano Res.* **2015**, *8*, 2415.

(11) (a) Dulle, J.; Thirunavukkarasu, K.; Mittelmeijer-Hazeleger, M. C.; Andreeva, D. V.; Shiju, N. R.; Rothenberg, G. *Green Chem.* **2013**, *15*, 1238. (b) Zhang, X.; Corma, A. *Angew. Chem., Int. Ed.* **2008**, *47*, 4358. (c) Borah, B. J.; Borah, S. J.; Saikia, L.; Dutta, D. K. *Catal. Sci. Technol.* **2014**, *4*, 1047. (d) Guo, H.; Liu, X.; Xie, Q.; Wang, L.; Peng, D. L.; Branco, P. S.; Gawande, M. B. *RSC Adv.* **2013**, *3*, 19812.

(12) (a) Tian, N.; Zhou, Z. Y.; Sun, S. G.; Ding, Y.; Wang, Z. L. *Science* **2007**, *316*, 732. (b) Huang, W. C.; Lyu, L. M.; Yang, Y. C.; Huang, M. H. *J. Am. Chem. Soc.* **2012**, *134*, 1261. (c) Zhang, H.; Jin, M.; Xia, Y. *Angew. Chem., Int. Ed.* **2012**, *51*, 7656. (d) Zhang, J.; Langille, M. R.; Personick, M. L.; Zhang, K.; Li, S.; Mirkin, C. A. *J. Am. Chem. Soc.* **2010**, *132*, 14012.

DOI: 10.1021/jacs.5b08289
J. Am. Chem. Soc. 2015, 137, 14027−14030